

Phosphorescence | Hot Paper |

Carboranes Tuning the Phosphorescence of Iridium Tetrazolate Complexes

Chao Shi,^[a] Deshuang Tu,^[a] Qi Yu,^[b] Hua Liang,^[b] Yahong Liu,^[b] Zhihong Li,^[a] Hong Yan,^{*,[a]} Qiang Zhao,^{*,[b]} and Wei Huang^{*,[b]}

Abstract: New iridium tetrazolate complexes containing *o*-, *m*-, or *p*-carboranyl substitution in different positions of a phenylpyridine ligand have been prepared. The carborane isomers and the effect of their substitution position in the tuning of optical properties have been examined. The neutral complexes with the carboranyl substituent on the phenyl ring in *meta* position relative to the metal exhibit redshifted emission bands in contrast to blueshifts for those with carboranyl in *para* position. All cationic complexes display evidently blueshifted dual-peak emission compared with the carborane-free complex (c-TZ) with a broad single-peak emission. Introduction of carborane leads to a blueshift

over 70 nm relative to c-TZ. Carboranes also significantly improve phosphorescence efficiency (Φ_p) and lifetime (τ), that is, $\Phi_p = 0.64$ versus 0.21 (c-TZ) and $\tau = 880$ ns versus 241 ns (c-TZ). The unique hydrophilic *nido*-carborane-based Ir^{III} complex *nido-o-1* shows the largest phosphorescence efficiency (abs $\Phi_p = 0.57$) among known water-soluble iridium complexes, long emission lifetime ($\tau = 4.38$ μ s), as well as varying emission efficiency and lifetime with O₂ content in aqueous solution. Therefore, *nido-o-1* has been used as an excellent oxygen-sensitive phosphor for intracellular O₂ sensing and hypoxia imaging.

Introduction

Icosahedral *closo*-carboranes including 1,2-, 1,7- and 1,12-C₂B₁₀H₁₂ (i.e., *o*-, *m*- and *p*-carborane) possess unusual three-dimensional pseudoaromatic geometric structures, which behave as bulky groups and exhibit unique push-pull electronic properties and thermal stability.^[1–5] On the basis of these advantages, recently, carboranes have been widely incorporated into organic^[6–15] and polymeric^[16–23] luminescent materials and have successfully tuned emission wavelength and luminescence efficiency. However, introduction of carboranes into phosphorescent transition-metal complexes has been less reported^[24–30] and mechanistic issues, such as how carboranes influence luminescence, have not been well addressed. We need to clarify the functions of carborane units on optical properties of metal complexes for further molecular design.

Current development of high-performance blue phosphorescent materials^[31–36] is urgently required for organic light-emitting

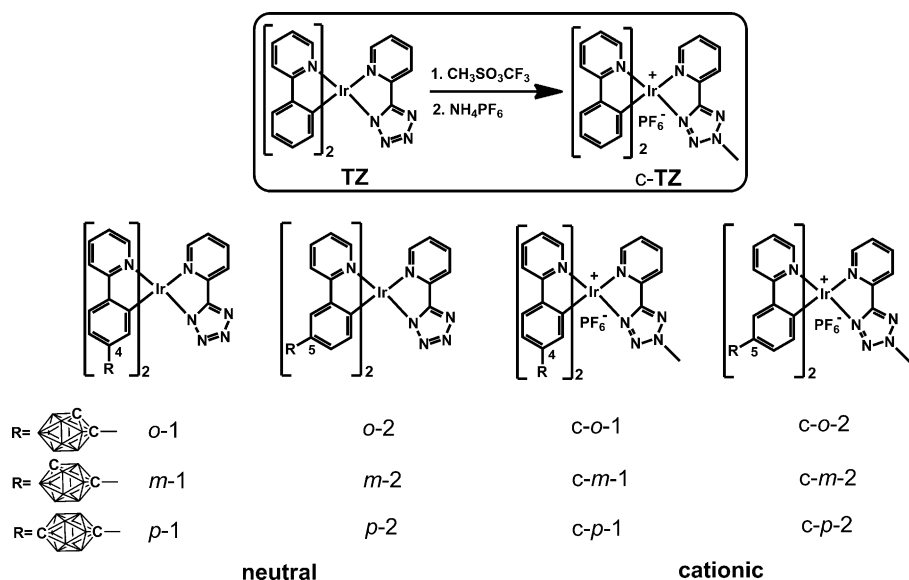
diodes (OLEDs). 2-Pyridyltetrazole is generally chosen as a N[^]N ligand to construct blue-emitting iridium complexes because it can both improve luminescence and lead to blueshifted emission of the target complexes.^[31] Besides, tetrazoles have been used as multidentate ligands that allowed to switch neutral to cationic complexes (Scheme 1), thus significantly tuning the optical properties of complexes.^[35] Moreover, hypoxia-sensitive imaging^[37–41] has attracted attention because hypoxia is a common feature of many diseases. However, most of the existing hypoxia probes are made from organic fluorescence dyes and phosphorescent transition-metal complexes.^[37–41] Hydrophobicity of these compounds is still a big problem. Phosphorescent iridium complexes have been extensively used in chemical sensing^[42–47] and living-cell imaging,^[48–52] because of the high luminescent efficiency, long phosphorescent lifetime, and tunable emission wavelength over the whole visible range. Therefore, to develop hydrophilic phosphorescent probes for detection of intracellular O₂ levels is of great significance for biological studies.

In this work, carboranes were introduced to pyridyltetrazolate iridium complexes TZ and c-TZ to synthesize neutral (*o*-1, *m*-1, *p*-1 and *o*-2, *m*-2, *p*-2) and cationic (c-*o*-1, c-*m*-1, c-*p*-1 and c-*o*-2, c-*m*-2, c-*p*-2) iridium derivatives containing *o*-, *m*- or *p*-carboranyl units in 4- or 5-position of phenyl ring of the cyclometalated C[^]N ligand (ppy) as shown in Scheme 1. We focused on revealing the effects of carboranes on the photo-physical properties of the new Ir complexes through the following aspects: 1) the effect of different carborane isomers; 2) the effect of the carboranyl group at different sites (4 or 5 position) of the C[^]N ligand; 3) the effect of the carboranyl

[a] C. Shi, D. Tu, Z. Li, Prof. Dr. H. Yan
State Key Laboratory of Coordination Chemistry
Nanjing University, Nanjing 210093 (P. R. China)
E-mail: hyan1965@nju.edu.cn

[b] Q. Yu, H. Liang, Y. Liu, Prof. Dr. Q. Zhao, Prof. Dr. W. Huang
Key Laboratory for Organic Electronics and Information Displays
and Institute of Advanced Materials
Nanjing University of Posts and Telecommunications
Nanjing 210046 (P. R. China)
E-mail: iamqzhao@njupt.edu.cn
iwei-huang@njupt.edu.cn

Supporting information for this article is available on the WWW under <http://dx.doi.org/10.1002/chem.201404743>.



Scheme 1. The structures of *closo*-carborane-functionalized neutral and cationic iridium tetrazolate complexes (top: synthesis of cationic complex c-TZ from the neutral complex TZ through methylation).

group on different structural type (neutral and cationic) of complexes. Carboranes can remarkably tune photophysical properties of these complexes. *o*-Carborane has the strongest influence, because it has the strongest electron-withdrawing ability among the three carborane isomers. The emission in *c-o-2* is blueshifted over 70 nm compared with the carborane-free complex (c-TZ), thus the emission color changes from yellow to blue. Phosphorescence efficiency (Φ_p) and lifetime (τ) have been improved 3–4 times ($\Phi_p=0.64$ for *o-1* relative to 0.21 for TZ and $\tau=880$ ns for *c-o-1* versus 241 ns for c-TZ). The carborane substitution site and the structural type of iridium complexes also have different impact on the photophysical properties, depending on the degrees of carborane-involved in excited state, as demonstrated by DFT studies. Also, hydrophilic *nido*-carborane-functionalized iridium complexes *nido-o-1* and *nido-o-2* have been prepared; the former shows the highest phosphorescence efficiency, with an absolute value of $\Phi_p=0.57$ in aqueous solution, among all known water-soluble iridium complexes and long phosphorescence lifetime ($\tau=4.38$ μs).^[29,53,54] The photophysical parameters are also quite sensitive to oxygen in both aqueous solution and in living cells. Thus, this *nido*-carborane-functionalized iridium complex might be promising in intracellular O_2 sensing and hypoxia imaging for biological system.

Results and Discussion

Synthesis and structure

Carborane-based cyclometalated ligands (4-R-ppy and 5-R-ppy) (ppy = phenylpyridine) were synthesized through the Suzuki–Miyaura cross-coupling reactions,^[55,56] by using 2-(6-phenyl-1,3,6,2-dioxazaborocan-2-yl)pyridine as a boron reagent, from the corresponding carborane-based precursors (4-R-Br and 5-R-Br) in yields of 80–85% (Scheme S1 in the Supporting Informa-

tion). The two types of chloro-bridged dimers $[(4\text{-R-ppy})_2\text{Ir}(\mu\text{-Cl})_2]$ and $[(5\text{-R-ppy})_2\text{Ir}(\mu\text{-Cl})_2]$ were prepared as reported by Nonoyama.^[57] Then a series of neutral carborane-based iridium tetrazolate complexes *o-1*, *m-1*, *p-1* and *o-2*, *m-2*, *p-2* were obtained by using 2-pyridyltetrazole as N^N ligand under mild conditions (at room temperature for 6–8 h). Reactions of the neutral complexes with stoichiometric amounts of methyltriflate led to the corresponding cationic complexes *c-o-1*, *c-m-1*, *c-p-1* and *c-o-2*, *c-m-2*, *c-p-2* (Scheme 1 and S1 in the Supporting Information). The two *nido*-carborane-functionalized iridium complexes *nido-o-1* and *nido-o-2* were obtained by de-

boronation from the corresponding *closo* derivatives *o-1* and *o-2* in boiling ethanol solution in quantitative yields (Scheme S2 in the Supporting Information).

All the new iridium complexes were identified by ^1H , ^{13}C , ^{11}B NMR spectroscopy, MS, and single-crystal X-ray crystallography. As shown in the solid-state structures of *o-1* and *o-2* (Figure 1), the iridium center adopts a distorted octahedral coordination geometry with *cis*-metalated carbons and *trans*-phenylpyridine nitrogen atoms, the same as previously observed

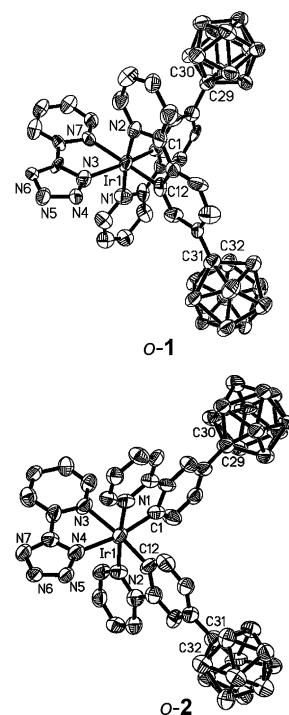


Figure 1. The crystal structures of *o-1* and *o-2*.

in other complexes containing the analogous cyclometalated C[^]N ligands.^[35] The Ir–N(N[^]N) distances (2.095–2.174 Å) are slightly longer than in Ir–N(C[^]N) (2.031–2.078 Å) because of the trans influence of the metalated carbon atoms (Figure S1 and S2 in the Supporting Information). Note that the two carborane cages are in the *para* position to the iridium atom in *o*-2, whereas in the *meta* position in *o*-1, which causes different polarity and electronic effects, as discussed latter by quantum chemical calculations.

Photophysical properties

The absorption and emission spectra of all complexes were measured at room temperature in dichloromethane (Figures 2,

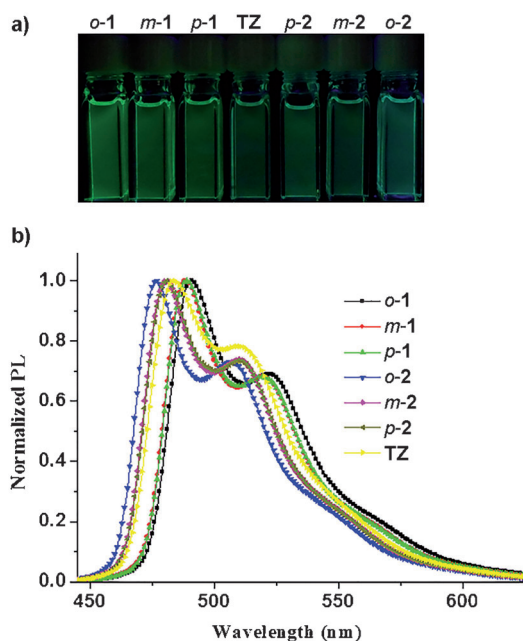


Figure 2. a) The luminescence photographs of all neutral complexes and b) the corresponding emission spectra in CH₂Cl₂.

3 and Table 1, see also the Supporting Information, Figures S3, S4, and Table S2). All carborane-based neutral complexes feature the intense absorption bands in the region of 250–360 nm, assigned to ¹π→π* transition of the ligand (¹LC) and show approximate redshift of 5 nm relative to the model complex TZ, due to the participation of carboranes in the extending π-conjugation (see calculated HOMO and LUMO in Figure S6 in the Supporting Information). The weak bands in the range of 350–450 nm are assigned to the metal-to-ligand charge-transfer transitions (¹MLCT and ³MLCT; Figure S3 in the Supporting Information). MLCT bands for *o*-1, *m*-1 and *p*-1 exhibit the obvious redshift in contrast to a blueshift for *o*-2, *m*-2 and *p*-2 (both referred to those in TZ). This indicates that the position of carborane substitution has influence on the ground- or excited-state energy.

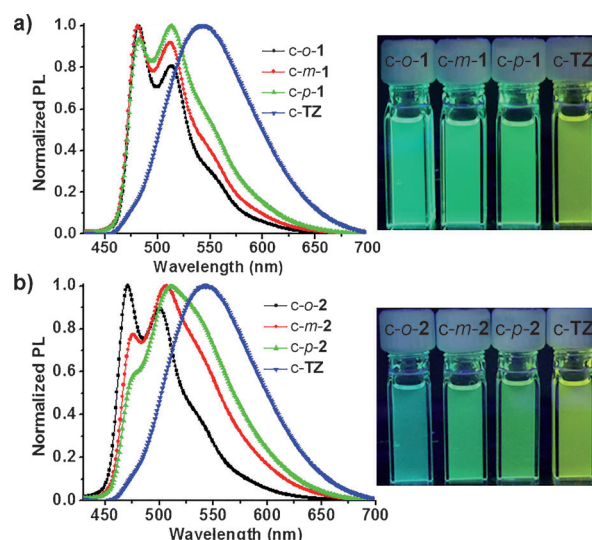


Figure 3. The emission spectra of cationic complexes a) *c*-*o*-1, *c*-*m*-1, *c*-*p*-1 and b) *c*-*o*-2, *c*-*m*-2, *c*-*p*-2, and *c*-TZ in CH₂Cl₂ and the corresponding luminescence photographs.

All the neutral complexes show dual emission peaks and also reflect the same trend in the excited-state energy (Figure 2 and Table 1). The emission peaks of *o*-1 (490 and 522 nm), *m*-1 (488 and 520 nm), and *p*-1 (488 and 520 nm) exhibit redshifts of 5–12 nm relative to those of TZ (483 and 510 nm). In contrast, *o*-2 (476 and 507 nm), *m*-2 (480 and 510 nm), and *p*-2 (480 and 510 nm) show blueshifts of 3–7 nm relative to those of TZ. The *o*-carborane substitution site modulates more evident changes in emission wavelength, about 14 nm from *o*-1 to *o*-2, thus the emission color tunes from green to blue-green (Figure 2). Moreover, carborane-substitution remarkably improves phosphorescence efficiency (Φ_p) owing to the rigidity of the carborane groups (Table 1), for example, $\Phi_p = 0.64$ for *o*-1 versus 0.21 for TZ.

In the cationic complexes, the introduction of carboranes has little effect on the absorption spectra (Figure S4 in the Supporting Information). However, the emission spectra are different. Firstly, all carborane-based cationic complexes display vibronic dual-peak emission in contrast to the broad single peak of the control complex *c*-TZ (Figure 3 and Table 1), demonstrating that the ligand-centered ³π→π* state (³LC) is more involved in the excited state of the carborane-based cationic complexes than it is in *c*-TZ. Secondly, all new cationic complexes exhibit an evident blueshift (29–71 nm) compared to *c*-TZ (542 nm), for example, *c*-*o*-2 (471 and 501 nm) has reached blueshifts of up to 71 nm. Correspondingly, the emission color changes from yellow for *c*-TZ to sky blue for *c*-*o*-2. Moreover, the carborane-substitution at C5 of the ppy ligand (see Scheme 1) leads to a slightly larger blueshift than that at C4 (Table 1). Thirdly, the carborane-based cationic complexes exhibit obvious blueshifts in comparison with the corresponding neutral complexes (that is, *c*-*o*-1 (481 and 513 nm) vs *o*-1 (490 and 522 nm)) in spite of a redshift from the neutral model complex TZ (483, 510 nm) to the cationic model complex *c*-TZ (542 nm). Complexes *c*-*o*-1, *c*-*m*-1, and *c*-*p*-1 display identical

emission wavelengths at 481 and 513 nm, but different relative intensities of the two peaks (Figure 3a), however, complexes *c-o-2*, *c-m-2*, and *c-p-2* show different emission wavelengths and intensities of the two peaks (Figure 3b). Furthermore, the peaks at about 510 nm of all cationic carborane-based complexes are broad in the order *c-o-1* < *c-m-1* < *c-p-1* and *c-o-2* < *c-m-2* < *c-p-2*, and the latter series of complexes show broader peaks. Therefore, the results demonstrate that carboranes can evidently tune emission spectra of pyridyltetrazolate iridium complexes in position, shape, phosphorescence efficiency, and lifetime (Table 1). Carborane isomers, carborane substitution sites, and structural types of complexes also have different impact on photophysical properties.

The electrochemical properties of all complexes were examined by cyclic voltammetry in acetonitrile solutions (Figure 4

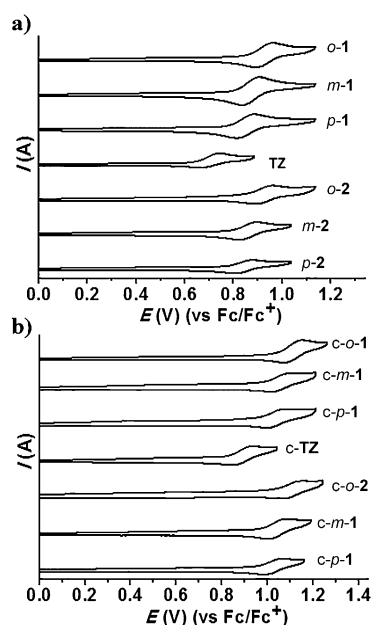


Figure 4. Cyclic voltammograms of a) neutral and b) cationic iridium tetrazolate complexes. Scan rate = 100 mV s⁻¹.

and Table 1). All complexes have reversible oxidation waves with potentials in the range of 0.6–1.3 V. The oxidation potentials of the cationic complexes show a positive shift of about 0.17 V in comparison with the corresponding neutral complexes, demonstrating that the latter are more easily oxidized. The values of oxidation potentials follow the order: *o-1* > *m-1* > *p-1* > *TZ*, *o-2* > *m-2* > *p-2* > *TZ*, *c-o-1* > *c-m-1* > *c-p-1* > *c-TZ*, and *c-o-2* > *c-m-2* > *c-p-2* > *c-TZ*, consistent with the order of electron-withdrawing ability of the carborane isomers. The results reveal that carboranes can increase oxidation potentials and reduce the energy level of HOMO (Table 1), as found in our previous reports.^[28,29] Carborane substitution in different positions does not affect the oxidation potential (i.e., $E_{\text{onset}} = 0.91$ V for *o-1* and $E_{\text{onset}} = 0.90$ V for *o-2*).

In attempt to explore potential applications of carborane-functionalized iridium complexes for biological systems, we modified the hydrophobic iridium tetrazolate complexes *TZ* by

	PL ^[a] [nm]	Φ_p ^[a]	τ ^[a] [ns]	$E_{\text{onset}}^{\text{ox}}$ [eV]	E_g ^[b] [eV]	HOMO/LUMO [eV] ^[b]
<i>o-1</i>	490, 522	0.64	747	0.91	2.66	-5.71/-2.99
<i>m-1</i>	488, 520	0.47	556	0.84	2.68	-5.64/-2.96
<i>p-1</i>	488, 520	0.43	479	0.83	2.68	-5.63/-2.95
<i>o-2</i>	476, 507	0.38	360	0.90	2.71	-5.70/-2.99
<i>m-2</i>	480, 510	0.36	338	0.83	2.70	-5.63/-2.93
<i>p-2</i>	480, 510	0.31	309	0.82	2.70	-5.62/-2.92
<i>TZ</i>	483, 510	0.21	207	0.68	2.69	-5.48/-2.79
<i>c-o-1</i>	481, 513	0.32	880	1.08	2.69	-5.88/-3.19
<i>c-m-1</i>	481, 513	0.16	410	1.02	2.68	-5.82/-3.14
<i>c-p-1</i>	481, 513	0.15	328	1.01	2.68	-5.81/-3.13
<i>c-o-2</i>	471, 501	0.25	530	1.07	2.71	-5.87/-3.16
<i>c-m-2</i>	475, 507	0.22	510	1.00	2.70	-5.80/-3.10
<i>c-p-2</i>	476, 509	0.21	495	0.99	2.70	-5.79/-3.09
<i>c-TZ</i>	542	0.19	241	0.86	2.62	-5.66/-3.04

[a] in CH₂Cl₂. [b] HOMO(eV) = -e($E_{\text{onset}}^{\text{ox}}$ + 4.8), $E_g = 1240/\lambda$, LUMO(eV) = E_g + HOMO.

introduction of a hydrophilic *nido-o*-carboranyl unit to prepare the water-soluble organometallic complexes *nido-o-1* and *nido-o-2* (Figure 5a and Scheme S2 in the Supporting Information). The ¹H NMR spectra show the characteristic broad B–H–B resonance of a *nido-o*-carboranyl unit. The ¹¹B NMR show less overlapped signals in a wider range, typical for a *nido-o*-carborane cage. The ESI-MS clearly demonstrate two peaks of $[M-K^+]^-$ and $[M-2K^+]^{2-}$. Both complexes display intense absorption

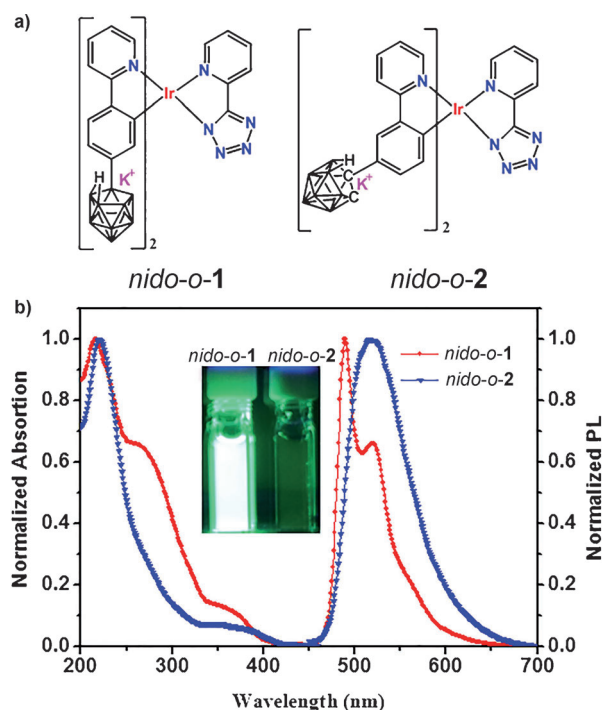


Figure 5. a) The structures of *nido*-carborane-functionalized iridium tetrazolate complexes and b) the absorption and PL spectra in aqueous solution (1.0×10^{-5} M). The inset shows the corresponding luminescence photographs.

bands below 400 nm, assigned to $^1\pi\rightarrow\pi^*$ transitions of the ligand (^1LC), but *nido-o-1* shows one additional peak at 270 nm. The weak bands in the range of 350–450 nm are likely attributed to metal-to-ligand charge-transfer transitions ($^1\text{MLCT}$, $^1\text{LLCT}$ and $^3\text{MLCT}$, $^3\text{LLCT}$; Figure 5b). Unexpectedly, the luminescent properties of both complexes are evidently different. Complex *nido-o-1* shows a vibronic dual-peak emission (489 and 520 nm) in contrast to a broader single-peak emission at 520 nm for *nido-o-2* (Figure 5b and Table S3 in the Supporting Information), demonstrating that the ^3LC state is more involved in excited-state in *nido-o-1* than in *nido-o-2*, as confirmed below by DFT calculations.

To our delight, *nido-o-1* exhibits exceptionally high phosphorescence efficiency with an absolute value of $\Phi_p=0.57$, the highest reported for water-soluble iridium complexes^[29,53,54] and long phosphorescence lifetime ($\tau=4.38\ \mu\text{s}$) in aqueous solution in sharp contrast to the very weak emission ($\Phi_p=0.08$) and shorter lifetime ($\tau=0.40\ \mu\text{s}$) for *nido-o-2* (Table S3 in the Supporting Information). This indicates that the *nido*-carborane substitution site has quite an impact on the emission. On the other hand, *nido-o-1* is highly sensitive to dioxygen in aqueous solutions (Figure 6). The emission intensity (I) and lifetime dra-

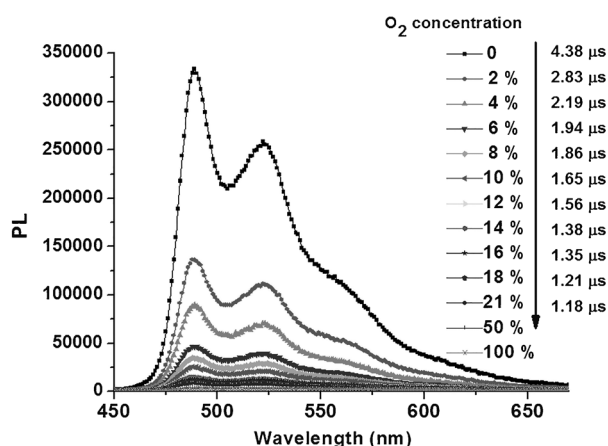


Figure 6. The change of emission spectra of *nido-o-1* ($1 \times 10^{-5}\ \text{M}$) in aqueous solution with different dioxygen concentrations.

matically reduces as the oxygen content increases, owing to energy transfer from the triplet excited state of *nido-o-1* to the triplet ground state of dioxygen. For instance, emission intensity and phosphorescence lifetime are decreased from $I=135822$, $\tau=2.83\ \mu\text{s}$ (2.0% O₂) to $I=8437$, $\tau=1.18\ \mu\text{s}$ (21% O₂).

Theoretical calculations

To elucidate the photophysical properties of all complexes discussed above, quantum chemical calculations were performed to gain insight into the structure–property relationships, including the functions of carboranes. As shown in Table S4 and Figure S5 in the Supporting Information, the calculated dipole moments of the ground states of all the complexes decrease as follows: $o-1 > p-1 > m-1$ or $c-o-1 > c-p-1 > c-m-1$, and $o-2 >$

$m-2 > p-2$ or $c-o-2 > c-m-2 > c-p-2$, indicating that the different carboranes and the substitution position cause evident difference in dipole moment of complexes led by the polarity competition between tetrazolate and carboranyl units. The data for the orbital analysis for all complexes are summarized in Figure 7, and in the Supporting Information in Figures S6, S7

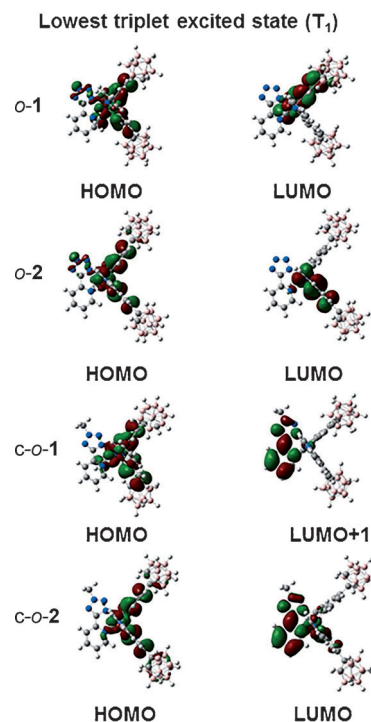


Figure 7. The optimized geometries of *o-1*, *o-2*, *c-o-1*, and *c-o-2* at the lowest triplet excited state (T_1).

and Tables S5–S7. The lowest energy absorption of all complexes is mainly characterized by a HOMO→LUMO transition. The HOMO is located on the iridium center and the phenyl ring of the C^{^N} ligand, but LUMO distribution depends on the complex types. In neutral complexes the LUMO is mainly located on the pyridyl and phenyl rings of the C^{^N} ligand, whereas in the cationic complexes, the LUMO distributes on the whole N^{^N} ligand (2-pyridyltetrazole). HOMO and LUMO energy levels descend with the incorporation of carboranes, and follow the order: $o-1 < m-1 < p-1 < \text{TZ}$, $c-o-1 < c-m-1 < c-p-1 < c-\text{TZ}$, and $o-2 < m-2 < p-2 < \text{TZ}$, $c-o-2 < c-m-2 < c-p-2 < c-\text{TZ}$, which is in agreement with the tendency revealed by experimental data.

The neutral and cationic complexes with carborane substitution in different positions show interesting optimized geometries of the lowest triplet excited state (T_1). Taking *o*-carborane derivatives as examples (Figure 7), the T_1 of both *o-1* and *o-2* are dominated by the HOMO→LUMO transition described as $^3\text{MLCT}$, $^3\text{ILCT}$, and ^3LC . Interestingly, the *o*-carborane cage partially participates in the LUMO (T_1), but is not involved in the HOMO for *o-1*. In *o-2*, however, the carborane unit is not involved in the LUMO (T_1), but partially participates in the HOMO (T_1). Thus the energy gap in *o-2* is larger than that in *o-1*, ex-

plaining well why *o*-2 shows an evident blueshifted emission compared with *o*-1. In the case of cationic complexes, the T_1 state of *c*-*o*-1 is dominated by HOMO→LUMO transitions with the character of $^3\text{MLCT}$ and $^3\text{LLCT}$, but by HOMO→LUMO+1 transitions in *c*-*o*-2 with the same character. The HOMO energy level (T_1) of *c*-*o*-2 is stabilized by a contribution from *o*-carborane, in contrast, no such contribution is found for *c*-*o*-1; thus the emission is more blueshifted in *c*-*o*-2 than in *c*-*o*-1. Similar trends were also observed in *m*- and *p*-carborane-based complexes (Table S7 in the Supporting Information).

In addition, the T_1 state of *nido*-*o*-1 originates from HOMO−1→LUMO+1 (0.58) and HOMO−1→LUMO (0.15) transitions with the respective character of $^3\text{LLCT}$ and ^3LC (Table S8 in the Supporting Information). The HOMO−1 is located on the C^N ligand, including the whole *nido*-carborane unit, whereas the LUMO only includes parts of the carborane unit. LUMO+1 resides on the whole N^N ligand (2-pyridyltetrazole; Figure 8). Complex *nido*-*o*-2, however, shows different T_1

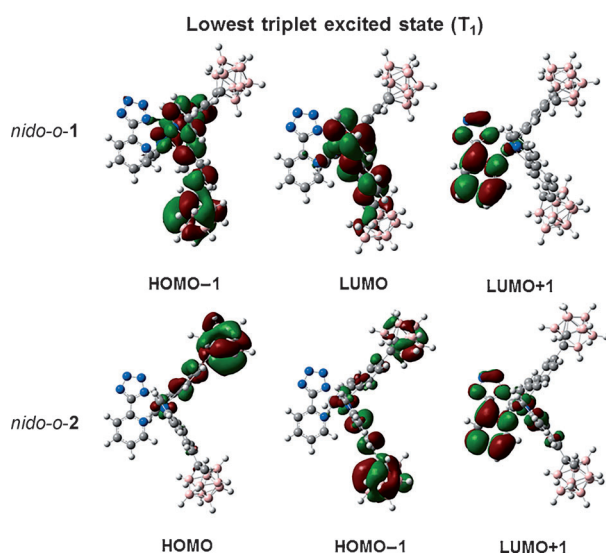


Figure 8. The optimized geometries of *nido*-*o*-1 and *nido*-*o*-2 at the lowest triplet excited state (T_1).

states, which arises from the transitions: HOMO→LUMO+1 (0.37) and HOMO−1→LUMO+1 (0.35) with one character of $^3\text{LLCT}$ (Table S8 in the Supporting Information). Both HOMO and HOMO−1 reside on the whole C^N ligand and LUMO+1 is located on the whole N^N ligand (2-pyridyltetrazole; Figure 8). It demonstrates that the ^3LC state is more involved in the excited state in *nido*-*o*-1 than in *nido*-*o*-2, consistent with the individual spectra.

Bioimaging

Because of the unique properties, such as excellent water solubility, high phosphorescence efficiency ($\Phi_p=0.57$), long phosphorescence lifetime ($\tau=4.38\ \mu\text{s}$), and emission sensitivity to dioxygen in aqueous solution, *nido*-*o*-1 is promising applications in hypoxia imaging. Firstly, the cytotoxicity towards

HepG2 liver cancer cells was evaluated by the MTT assay. After treatment of the cancer cells with different concentrations of *nido*-*o*-1 for 48 h, the cellular viabilities were estimated to be more than 80% even at 100 μM , and no cytotoxicity was observed at 10 μM (Figure S8 in the Supporting Information), which is the concentration that was used for imaging experiments in this study.

We then used *nido*-*o*-1 as a probe to detect intracellular oxygen levels in HepG2 cells, which were cultured with 21% or 2.5% O_2 concentration for 24 h at 37 °C. Complex *nido*-*o*-1 (10 μM) was added to the medium and the cells were incubated for two hours after washing with phosphate-buffered saline (PBS) in a 21% or 2.5% O_2 atmosphere. The excitation wavelength was 405 nm. Figure 9A shows the emission

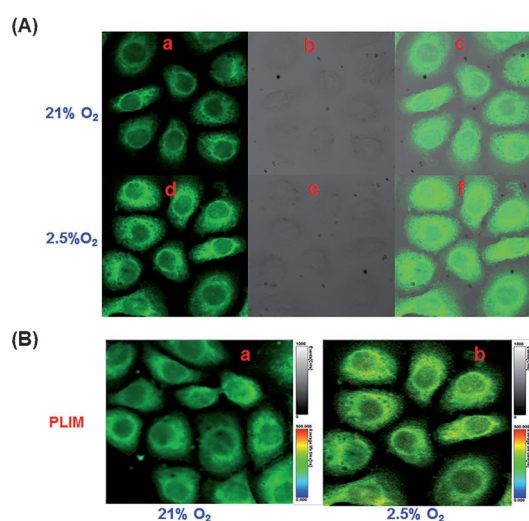


Figure 9. A) Phosphorescent images (a, d), bright-field images (b, e), overlay images (c, f) and B) phosphorescence lifetime images (a, b) of HepG2 live cells incubated with *nido*-*o*-1 (10 μM) in PBS at 37 °C with different O_2 content (21 and 2.5%) and excitation at 405 nm.

images of the living cells observed in the wavelength range 450–550 nm. We found that *nido*-*o*-1 was efficiently taken up by HepG2 cells. From overlays of bright-field images and confocal luminescence images, the luminescence was localized in the cytoplasm at the nucleus and the membrane (Figure 9A (c, f)), indicating that *nido*-*o*-1 is internalized into the cells. The image is brighter for cells exposed to 2.5% O_2 than for those exposed to 21% O_2 , demonstrating that *nido*-*o*-1 may be used to indicate intracellular oxygen concentrations. Additionally, considering the long phosphorescence lifetime, which is sensitive to dioxygen, lifetime-imaging experiments with both 21% and 2.5% O_2 concentrations were also conducted. As a result, high-quality long emission lifetime signals were observed (Figure 9B (a, b)) and the lifetime was significantly increased from 260 ns (21% O_2) to 380 ns (2.5% O_2) along with a visually distinct color change from green to yellow. Thus *nido*-*o*-1 might be a potential agent for hypoxia imaging by using both emission intensity and lifetime as sensing signals.

Conclusion

Carboranes have been successfully introduced into phosphorescent iridium tetrazolate complexes; this efficiently tuned the photophysical properties of this type of complexes. The photophysical properties depend on structural variations of the carboranes, the substitution site of the carboranes, and the structure of the iridium complexes. The maximum emission wavelength can be tuned by 71 nm with the emission color changing from yellow to blue. The phosphorescence efficiency and lifetime can be improved approximately 3–4 times. Incorporation of a hydrophilic *nido*-carborane leads to the water-soluble organometallic phosphorescent iridium complex *nido-o-1*, which has excellent phosphorescence efficiency ($\Phi_p=0.57$), long phosphorescence lifetime ($\tau=4.38\ \mu\text{s}$), variable phosphorescence efficiency and lifetime with O_2 content in aqueous solution, and low cytotoxicity. Thus, *nido-o-1* was used for O_2 sensing and bioimaging in living cells. These results are helpful for further design of desired carborane-functionalized, phosphorescent, metal complexes for optoelectronic and biological applications.

Experimental Section

General: All air- and moisture-sensitive reactions were carried out under an argon atmosphere. Dry 1,2-dimethoxyethane and pyridine were obtained by refluxing and distilling over CaH_2 under nitrogen. Dry THF was distilled from sodium/benzophenone. *n*BuLi (2.4 M in hexanes, Amethyst) was used as supplied. $[(4\text{-R-ppy})_2\text{Ir}(\mu\text{-Cl})_2]$ (R = *o*-, *m*- or *p*-carboranyl)^[28] were synthesized according to literature procedures. The ^1H , ^{13}C and ^{11}B NMR spectra were measured at room temperature with a Bruker DRX-500 or a Bruker DRX-600 spectrometer. Mass spectra were measured with a Micromass GC-TOF for EI-MS (70 eV) and an ESI-MS (LCQ Fleet, Thermo Fisher Scientific). Infrared spectra were determined by a Nicolet NEXUS870 FTIR spectrometer. Electrochemical measurements were performed with an IM6ex instrument (Zahner). Phosphorescence spectral measurements were carried out by using a Hitachi F-4600 fluorescence spectrophotometer. Electronic absorption spectra were recorded with Shimadzu UV-2550 spectrophotometer. Phosphorescence lifetimes were determined by an Edinburgh instrument laser impulse fluorimeter with picosecond time resolution. Elemental analyses for C, H, and N were performed on a Vario MICRO elemental analyzer.

Quantum yield determinations: Phosphorescence spectroscopic studies were performed on a Hitachi F-4600 fluorescence spectrophotometer and a Shimadzu UV-2550 spectrophotometer. The absolute quantum yields of phosphorescence of all complexes were determined by employing an integrating sphere. Lifetime studies were performed with an Edinburgh FL 920 photcounting system with a hydrogen-filled lamp as the excitation source.

Electrochemical measurements: Cyclic voltametric experiments were carried out with an IM6ex instrument (Zahner) using three electrode cell assemblies. All measurements were carried out in a one-compartment cell under Argon, equipped with a glassy-carbon working electrode, a platinum wire counter electrode, and a Ag/Ag^+ reference electrode with a scan rate of $100\ \text{mV s}^{-1}$. The supporting electrolyte was a $0.10\ \text{mol L}^{-1}$ acetonitrile solution of tetrabutylammonium hexafluorophosphate (Bu_4NPF_6). Each oxidation potential was calibrated with ferrocene as reference.

Quantum chemical calculations: The geometries of all iridium(III) complexes were optimized with the DFT method. The electronic transition energies, including electron correlation effects, were computed by the time-dependent (TD)-DFT method using the B3LYP functional (TD-B3LYP). The LANL2DZ basis set was used to treat the iridium atom, whilst the 6–31G(d) basis set was used to treat all other atoms. All calculations described here were performed by using the Gaussian 09 program.^[58]

Confocal luminescence imaging and phosphorescence lifetime imaging (PLIM): Confocal luminescence imaging was carried out on an Olympus IX81 laser scanning confocal microscope equipped with a 40 immersion objective lens. A semiconductor laser served as the excitation source of the HepG2 liver cancer cells incubated with *nido-o-1* at 405 nm. The one-photon emission was collected at 450–550 nm for the HepG2 liver cancer cells incubated with *nido-o-1*. Complex *nido-o-1* was added to RPMI 1640 to yield a $10\ \mu\text{M}$ solution. The HepG2 liver cancer cells were incubated with the solution of *nido-o-1* with 20% or 2.5% O_2 for 2 h at $37\ ^\circ\text{C}$.

The FLIM image setup was integrated with an Olympus IX81 laser scanning confocal microscope. The fluorescence signal was detected by the system of the confocal microscope and correlative calculation of the data was performed with professional software, which was provided by PicoQuant. The light from the pulse diode laser head (PicoQuant, PDL 800-D), with an excitation wavelength of 405 nm and a frequency of 0.5 MHz, was focused onto the sample with a 40x/NA 0.95 objective lens for single-photon excitation. The emitted fluorescence signal was collected at 450–550 nm.

Acknowledgements

Financial support from the National Natural Science Foundation of China (21271102), the Natural Science Foundation of Jiangsu Province of China (BK20130038 and BK20130054), the Major State Basic Research Development Program of China (2013CB922100) and the High-Performance Computational Centre of Nanjing University is acknowledged.

Keywords: bioimaging · carboranes · iridium · phosphorescence

- [1] A. M. Spokoyny, C. W. Machan, D. J. Clingerman, M. S. Rosen, M. J. Wiestner, R. D. Kennedy, C. L. Stem, A. A. Sarieant, C. A. Mirkin, *Nature Chem.* **2011**, *3*, 590.
- [2] R. E. Williams, *Chem. Rev.* **1992**, *92*, 117.
- [3] V. I. Bregadze, *Chem. Rev.* **1992**, *92*, 209.
- [4] M. F. Hawthorne, A. Maderna, *Chem. Rev.* **1999**, *99*, 3421.
- [5] R. N. Grimes, *Carboranes*, Vol. 9, 2nd ed., Academic Press, New York, **2011**, pp. 301–540.
- [6] B. P. Dash, R. Satapathy, J. A. Maguire, N. S. Hosmane, *New J. Chem.* **2011**, *35*, 1955.
- [7] B. P. Dash, R. Satapathy, E. R. Gaillard, K. M. Norton, J. A. Maguire, N. Chug, N. S. Hosmane, *Inorg. Chem.* **2011**, *50*, 5485.
- [8] K. Kokado, Y. Chujo, *J. Org. Chem.* **2011**, *76*, 316.
- [9] Y. Morisaki, M. Tominaga, Y. Chujo, *Chem. Eur. J.* **2012**, *18*, 11251.
- [10] K. R. Wee, W. S. Han, D. W. Cho, S. Kwon, C. Pac, S. O. Kang, *Angew. Chem. Int. Ed.* **2012**, *51*, 2677; *Angew. Chem.* **2012**, *124*, 2731.
- [11] K. R. Wee, Y. J. Cho, S. Jeong, S. Kwon, J. D. Lee, I. H. Suh, S. O. Kang, *J. Am. Chem. Soc.* **2012**, *134*, 17982.
- [12] L. Weber, J. Kahlert, R. Brockhinke, L. Bohling, A. Brockhinke, H. G. Stammer, B. Neumann, R. A. Harder, M. A. Fox, *Chem. Eur. J.* **2012**, *18*, 8347.
- [13] A. Ferrer Ugalde, E. José, J. Pérez, F. Teixidor, C. Viñas, R. Sillanpää, E.-P. Inestrosa, R. Núñez, *Chem. Eur. J.* **2012**, *18*, 544.

- [14] A. Harriman, M. A. H. Alamiry, J. P. Hagon, D. Hablot, R. Ziessel, *Angew. Chem. Int. Ed.* **2013**, *52*, 6611; *Angew. Chem.* **2013**, *125*, 6743.
- [15] L. Zhu, W. Lv, S. Liu, H. Yan, Q. Zhao, W. Huang, *Chem. Commun.* **2013**, *49*, 10638.
- [16] K. Kokado, Y. Tokoro, Y. Chujo, *Macromolecules* **2009**, *42*, 9238.
- [17] K. Kokado, Y. Tokoro, *Macromolecules* **2009**, *42*, 1418.
- [18] K. Kokado, Y. Tokoro, Y. Chujo, *Macromolecules* **2009**, *42*, 2925.
- [19] K. Kokado, M. Tominaga, Y. Chujo, *Macromol. Rapid Commun.* **2010**, *31*, 1389.
- [20] Y. C. Simon, J. J. Peterson, C. Mangold, K. R. Carter, E. B. Coughlin, *Macromolecules* **2009**, *42*, 512.
- [21] J. J. Peterson, M. Werre, Y. C. Simon, E. B. Coughlin, K. R. Carter, *Macromolecules* **2009**, *42*, 8594.
- [22] J. J. Peterson, Y. C. Simon, E. B. Coughlin, K. R. Carter, *Chem. Commun.* **2009**, 4950.
- [23] A. R. Davis, J. J. Peterson, K. R. Carter, *ACS Macro Lett.* **2012**, *1*, 469.
- [24] A. M. Prokhorov, P. A. Slepukhin, V. L. Rusinov, V. N. Kalinin, D. N. Kozhevnikov, *Chem. Commun.* **2011**, *47*, 7713.
- [25] T. Kim, H. Kim, K. M. Lee, Y. S. Lee, M. H. Lee, *Inorg. Chem.* **2013**, *52*, 160.
- [26] H. G. Bae, J. Chung, H. Kim, J. Park, K. M. Lee, T. W. Koh, Y. S. Lee, S. Yoo, Y. Do, M. H. Lee, *Inorg. Chem.* **2014**, *53*, 128.
- [27] R. Visbal, I. Ospino, J. M. López-de-Luzuriaga, A. Laguna, M. C. Gimeno, *J. Am. Chem. Soc.* **2013**, *135*, 4712.
- [28] C. Shi, H. B. Sun, Q. B. Jiang, Q. Zhao, J. X. Wang, W. Huang, H. Yan, *Chem. Commun.* **2013**, *49*, 4746.
- [29] C. Shi, H. B. Sun, X. Tang, W. Lv, H. Yan, Q. Zhao, J. Wang, W. Huang, *Angew. Chem. Int. Ed.* **2013**, *52*, 13434; *Angew. Chem.* **2013**, *125*, 13676.
- [30] A. M. Prokhorov, T. Hofbeck, R. Czerwieńiec, A. F. Suleymanova, D. N. Kozhevnikov, H. Yersin, *J. Am. Chem. Soc.* **2014**, *136*, 9637.
- [31] S. J. Yeh, M. F. Wu, C. T. Chen, Y. H. Song, Y. Chi, M. H. Ho, S. F. Hsu, C. H. Chen, *Adv. Mater.* **2005**, *17*, 285.
- [32] C. H. Yang, Y. M. Cheng, Y. Chi, C. J. Hsu, F. C. Fang, K. T. Wong, P. T. Chou, C. H. Chang, M. H. Tsai, C. C. Wu, *Angew. Chem. Int. Ed.* **2007**, *46*, 2418; *Angew. Chem.* **2007**, *119*, 2470.
- [33] C. F. Chang, Y. M. Cheng, Y. Chi, Y. C. Chiu, C. C. Lin, G. H. Lee, P. T. Chou, C. C. Chen, C. H. Chang, C. C. Wu, *Angew. Chem. Int. Ed.* **2008**, *47*, 4542; *Angew. Chem.* **2008**, *120*, 4618.
- [34] K. Y. Lu, H. H. Chou, C. H. Hsieh, Y. H. O. Yang, H. R. Tsai, H. Y. Tsai, L. C. Hsu, C. Y. Chen, I. C. Chen, C. H. Cheng, *Adv. Mater.* **2011**, *23*, 4933.
- [35] S. Stagni, S. Colella, A. Palazzi, G. Valenti, S. Zacchini, F. Paolucci, M. Marzaccio, R. Q. Albuquerque, L. D. Cola, *Inorg. Chem.* **2008**, *47*, 10509.
- [36] X. N. Li, Z. J. Wu, Z. J. Si, H. J. Zhang, L. Zhou, X. J. Liu, *Inorg. Chem.* **2009**, *48*, 7740.
- [37] K. Kiyose, K. Hanaoka, D. Oshiki, T. Nakamura, M. Kajimura, M. Suematsu, H. Nishimatsu, T. Yamane, T. Terai, Y. Hirata, T. Nagano, *J. Am. Chem. Soc.* **2010**, *132*, 15846.
- [38] S. Takahashi, W. Piao, Y. Matsumura, T. Komatsu, T. Ueno, T. Terai, T. Kamachi, M. Kohno, T. Nagano, K. Hanaoka, *J. Am. Chem. Soc.* **2012**, *134*, 19588.
- [39] T. Yoshihara, Y. Yamaguchi, M. Hosaka, T. Takeuchi, S. Tobita, *Angew. Chem. Int. Ed.* **2012**, *51*, 4148; *Angew. Chem.* **2012**, *124*, 4224.
- [40] W. Piao, S. Tsuda, Y. Tanaka, S. Maeda, F. Liu, S. Takahashi, Y. Kushida, T. Komatsu, T. Ueno, T. Terai, T. Nakazawa, M. Uchiyama, K. Morokuma, T. Nagano, K. Hanaoka, *Angew. Chem. Int. Ed.* **2013**, *52*, 13028; *Angew. Chem.* **2013**, *125*, 13266.
- [41] R. Dubey, M. D. Levin, L. Z. Szabo, C. F. Laszlo, S. Kushal, J. B. Singh, P. Oh, J. E. Schnitzer, B. Z. Olenyuk, *J. Am. Chem. Soc.* **2013**, *135*, 4537.
- [42] Q. Zhao, F. Y. Li, C. H. Huang, *Chem. Soc. Rev.* **2010**, *39*, 3007.
- [43] Y. You, Y. Han, Y. M. Lee, S. Y. Park, W. Nam, S. J. Lippard, *J. Am. Chem. Soc.* **2011**, *133*, 11488.
- [44] H. Shi, H. Sun, H. Yang, S. Liu, G. Jenkins, W. Feng, F. Li, Q. Zhao, B. Liu, W. Huang, *Adv. Funct. Mater.* **2013**, *23*, 3268.
- [45] W. Xu, S. Liu, X. Zhao, N. Zhao, Z. Liu, H. Xu, H. Liang, Q. Zhao, X. Yu, W. Huang, *Chem. Eur. J.* **2013**, *19*, 621.
- [46] W. Xu, S. Liu, X. Zhao, S. Sun, S. Cheng, T. Ma, H. Sun, Q. Zhao, W. Huang, *Chem. Eur. J.* **2010**, *16*, 7125.
- [47] H. Sun, S. Liu, W. Lin, K. Y. Zhang, W. Lv, X. Huang, F. Huo, H. Yang, G. Jenkins, Q. Zhao, W. Huang, *Nature Commun.* **2014**, *5*, 3601.
- [48] D. L. Ma, W. L. Wong, W. H. Chung, F. Y. Chan, P. K. So, T. S. Lai, Z. Y. Zhou, Y. C. Leung, K. Y. Wong, *Angew. Chem. Int. Ed.* **2008**, *47*, 3735; *Angew. Chem.* **2008**, *120*, 3795.
- [49] Q. Zhao, C. H. Huang, F. Y. Li, *Chem. Soc. Rev.* **2011**, *40*, 2508.
- [50] W. Xu, X. Zhao, W. Lv, H. Yang, S. Liu, H. Liang, Z. Tu, H. Xu, W. Qiao, Q. Zhao, W. Huang, *Adv. Healthcare Mater.* **2014**, *3*, 658.
- [51] C. Li, M. Yu, Y. Sun, Y. Wu, C. Huang, F. Li, *J. Am. Chem. Soc.* **2011**, *133*, 11231.
- [52] X. Liu, N. Xi, S. Liu, Y. Ma, H. Yang, H. Li, J. He, Q. Zhao, F. Li, W. Huang, *J. Mater. Chem.* **2012**, *22*, 7894.
- [53] Y. Ma, S. Liu, H. Yang, Y. Wu, C. Yang, X. Liu, Q. Zhao, H. Wu, J. Liang, F. Li, W. Huang, *J. Mater. Chem.* **2011**, *21*, 18974.
- [54] Y. Ma, S. Liu, H. Yang, Y. Wu, H. Sun, J. Wang, Q. Zhao, F. Li, W. Huang, *J. Mater. Chem. B* **2013**, *1*, 319.
- [55] P. B. Hodgson, F. H. Salingue, *Tetrahedron Lett.* **2004**, *45*, 685.
- [56] C. Gutz, A. Lutzen, *Synthesis* **2010**, *1*, 85.
- [57] M. Nonoyama, *Bull. Chem. Soc. Jpn.* **1974**, *47*, 767.
- [58] Gaussian 09, Revision B.01, M. J. Frisch, G. W. Trucks, H. B. Schlegel, G. E. Scuseria, M. A. Robb, J. R. Cheeseman, G. Scalmani, V. Barone, B. Menonucci, G. A. Petersson, H. Nakatsuji, M. Caricato, X. Li, H. P. Hratchian, A. F. Izmaylov, J. Bloino, G. Zheng, J. L. Sonnenberg, M. Hada, M. Ehara, K. Toyota, R. Fukuda, J. Hasegawa, M. Ishida, T. Nakajima, Y. Honda, O. Kitao, H. Nakai, T. Vreven, J. A. Montgomery, Jr., J. E. Peralta, F. Ogliaro, M. Bearpark, J. J. Heyd, E. Brothers, K. N. Kudin, V. N. Staroverov, R. Kobayashi, J. Normand, K. Raghavachari, A. Rendell, J. C. Burant, S. S. Iyengar, J. Tomasi, M. Cossi, N. Rega, J. M. Millam, M. Klene, J. E. Knox, J. B. Cross, V. Bakken, C. Adamo, J. Jaramillo, R. Gomperts, R. E. Stratmann, O. Yazyev, A. J. Austin, R. Cammi, C. Pomelli, J. W. Ochterski, R. L. Martin, K. Morokuma, V. G. Zakrzewski, G. A. Voth, P. Salvador, J. J. Dannenberg, S. Dapprich, A. D. Daniels, Ö. Farkas, J. B. Foresman, J. V. Ortiz, J. Cio-slowski, D. J. Fox, Gaussian, Inc., Wallingford CT, **2009**.

Received: August 5, 2014

Published online on October 28, 2014